Published in *Physics in Canada*, Oct 1997, see also http://mobydick.physics.utoronto.ca

Pattern formation in smectic liquid crystal films

John R. de Bruyn

Department of Physics, Memorial University of Newfoundland, St. John's, Newfoundland, Canada A1B 3X7

Stephen W. Morris

Department of Physics and Erindale College, University of Toronto, 60 St. George St., Toronto, Ontario, Canada M5S 1A7

(October 13, 1997)

Abstract

Many initially uniform systems can develop regular patterns of spatial structure when driven sufficiently far from equilibrium. In their simplest forms, these patterns resemble soft condensed phases. Pattern formation takes place via instabilities that are the nonequilibrium equivalent of phase transitions. We first provide a general overview of the study of pattern formation in fluid dynamical systems. We then describe recent experimental and theoretical work on patterns formed by electrically driven convection in very thin, freely-suspended films of smectic liquid crystals.

I. INTRODUCTION

Most of the typical undergraduate (and graduate) physics curriculum involves equilibrium, linear systems, and most of us are used to thinking *linearly*: small changes should produce correspondingly small effects; the principle of superposition should apply. We are trained to expect systems to seek, and be found in, equilibrium. In contrast, many real world phenomena occur far from equilibrium and are extremely nonlinear. The weather is unpredictable more than a few days in advance; bridges collapse suddenly; fish stocks disappear; straws can break the backs of camels. The behaviour of typical soft condensed matter systems may seem remote from such phenomena, but, perhaps surprisingly, we can construct a bridge between the two. Traversing this bridge has taken many of us who formerly thought of ourselves as pure condensed matter physicists into exciting new territories. The phenomenon of nonequilibrium pattern formation [1] forms this bridge.

Nonequilibrium patterns have been studied scientifically for at least 150 years. Perhaps the most-studied example is that of convection cells in a layer of fluid heated from below. When the temperature difference across the fluid layer is smaller than some critical value, there is no flow in the fluid, and all of the heat is transported across the layer by thermal conduction. At a critical temperature difference, however, an organized flow pattern develops. This system is known as Rayleigh-Bénard convection, and the onset of convection is an example of a pattern-forming hydrodynamic instability. The pattern is a macroscopically ordered structure that only exists away from equilibrium, yet displays behaviour which is strongly analogous to that of a simple, rather soft, ordered phase. Indeed, the analogy between the onset of the flow pattern and an equilibrium phase transition is nearly exact, as we discuss below.

If the convecting fluid layer is thin and its upper surface is open to the air, the pattern that forms is a periodic array of hexagonal convection cells. This pattern was the subject of Bénard's original studies around the turn of the century, using whale oil as the working fluid. In later experiments, the top and bottom of the layer were in contact with hot and

cold rigid boundaries. In that case, one finds instead that a periodic pattern of long, straight convective rolls forms. From this brief description it is already evident that we might expect rather complicated behaviour in this system, as convection patterns of completely different symmetries can develop, depending on the boundary conditions, or more generally on the symmetries of the experimental system. Just above the onset of convection, depending on the experimental conditions, one can observe bistability and competition between hexagonal and straight-roll patterns. Many features of these patterns and the transitions between them resemble their counterparts in soft condensed systems. For example, similar defect structures are found. Many of the theoretical and experimental tools and techniques used in the study of equilibrium phases and phase transitions may be carried over to the study of these patterns. However, patterns are ultimately generated by nonlinearities in the governing equations, and many new phenomena arise. As one moves father from the onset of convection, the full complexity is gradually realized: higher instabilities of the patterns generally lead to time dependence, spatio-temporal chaos, and ultimately turbulence. Thus, one can smoothly cross a bridge between familiar orderly behaviour and the most general and difficult to understand dynamical states. Pattern formation is one manifestation of nonlinearity, and the study of patterns is one branch of what has become known as nonlinear science [2].

Simple patterns are observed in many other nonequilibrium systems. A variety of spatial patterns as well as complex temporal behaviour have been studied in systems involving chemical reactions [3]. Icicles can form in long, periodically spaced arrays [4]. Rocks show spatial oscillations in their chemical composition [5], and amoebae exhibit spatiotemporal patterns in their chemical signaling [6]. Fluid mechanical systems have been particularly well studied, for two reasons. First, it is possible to do experiments with fluids in which the fluid properties, the boundary conditions, and the experimental conditions are all extremely well controlled. Second, the equations which describe fluid systems are similarly well-known. This allows for the possibility of close contact between experiment, analytical theory, and numerical computation in these systems. In the case of Rayleigh-Bénard convection, this contact is impressive and quantitative [1,7].

In the remainder of this, paper we discuss pattern formation in general, and then focus on a particular system — electroconvection in freely suspended fluid films — which we are studying. In section II we introduce the subject of pattern forming hydrodynamic instabilities in more detail and outline some simple theoretical approaches to the study of pattern formation. We also highlight the interesting open questions in the field. Then in section III, we describe our own work on electroconvection patterns in smectic liquid crystal films. [8–13] Smectic liquid crystals are themselves an example of a soft condensed matter system. We discuss how their unique properties allow us to do experiments on an almost perfect two-dimensional fluid and describe our experimental and theoretical work in relation to the discussion of section II. The paper ends with a brief discussion. An annotated list of helpful introductory references is provided in an Appendix.

II. PATTERN FORMATION IN FLUIDS

Why do patterns form? For concreteness we will consider Rayleigh-Bénard convection, but our arguments will be quite general and will be applied to the case of electroconvection patterns in smectic films in section III. Consider a thin horizontal layer of water, heated from below. Because the water has a finite thermal conductivity, it will be hotter at the bottom of the layer, and cooler at the top, and thermal expansion will cause it to be more dense on top than at the bottom. This is not the most stable configuration of the fluid; the system would have a lower gravitational potential energy if the heavy fluid were at the bottom and the light fluid on top. The problem is that to make the switch, the fluid has to flow. Flow requires energy because of viscous dissipation, and there is no point in trying to move the cold, heavy fluid down to the bottom of the layer unless the reduction in gravitational potential energy more than compensates for the energy losses due to viscosity. The finite thermal conductivity also hinders the motion: any parcel of cold fluid which moves down will be heated by the surrounding warm fluid and decrease its density, which reduces its loss in potential energy. Thus, our fluid layer is stable for small values of the temperature difference

across it, even though the density profile is inverted. When the temperature difference gets large enough, however, convective flow will begin. We expect a transition from the no-flow state to a state with convective flow when the temperature difference becomes large enough.

Other pattern-forming instabilities have similar origins: A competition between different processes leads to a qualitative change in the system as the relative importance of the processes changes.

The convective flow pattern which appears in an experiment is periodic with a characteristic wavelength. This can also be understood in terms of a competition between gains in gravitational potential energy and dissipation. A flow pattern involving many convection rolls, with lateral length scales very small compared to the thickness of the layer, would efficiently transport fluid from one boundary of the layer to the other, but would dissipate large amounts of energy because of the many regions of large shear in the fluid. Similarly, such a high periodicity would be hard to sustain against thermal conduction because of the closely spaced hot and cold regions created. In contrast, a small number of rolls with a wavelength large compared to the layer depth would reduce viscous and thermal losses, but give less efficient mass transport. The optimum roll width is somewhere in the middle, on the order of the layer thickness. The precise value of the wavelength depends on the details of the boundary conditions at the top and bottom of the layer. In other pattern-forming systems, the periodicity of the pattern is determined by similar trade-offs between driving forces and dissipation.

We can get some information about the onset of the flow pattern by looking at the stability of the no-flow state. One can, of course, numerically solve the well-known equations of fluid mechanics, the Navier-Stokes equations, and reproduce the phenomena quite well. Much more insight, and a more universal description, can be obtained with simpler equations, however. As an example, consider the equation

$$\dot{A} = \epsilon A - gA^3. \tag{1}$$

Here A describes the slowly-varying amplitude, or envelope, of the flow pattern in the fluid,

the dot represents differentiation with respect to time, and g is a positive constant. ϵ is our control parameter, corresponding to the temperature difference in Rayleigh-Bénard convection. This simplified model equation is more than just illustrative; with slight modifications it can be derived from the full Navier-Stokes equations for Rayleigh-Bénard convection close to the convective onset.

Let us look for steady-state solutions of Eq. 1, that is, solutions for which $\dot{A} = 0$. There is always a solution with $A = 0$, corresponding to a state with no flow, and for $\epsilon < 0$ it is the only real solution. However for $\epsilon > 0$ there are two more solutions, given by $A = \pm(\epsilon/g)^{1/2}$. There is thus a qualitative change in the character of the solutions to Eq. 1 at $\epsilon = 0$, corresponding to the appearance of the flow pattern. This change is called a bifurcation, and $\epsilon = 0$ is the bifurcation point.

Now let's study the stability of these solutions. We do this by adding a small perturbation to the steady-state solutions, substituting the perturbed solution into Eq. 1, and seeing whether the perturbations grow or die away with time. In the former case, the steady-state solution is unstable to small perturbations, while in the latter case it is stable.

For the $A = 0$ state, our perturbed solution is $A = 0 + a(t)$, where a is small. Substituting this into Eq. 1 gives an equation for the evolution of $a(t)$. To linear order in the small quantity a this is

$$\dot{a} = \epsilon a \tag{2}$$

from which we see that the no flow state is stable (the perturbations die away) if $\epsilon < 0$, and unstable if $\epsilon > 0$. Since the no flow state becomes unstable at the bifurcation point, we might suspect that the two new solutions which appear there are stable. To test this, we write the perturbed forms of the new solutions as $A = A_0 + a(t)$, where $A_0 = (\epsilon/g)^{1/2}$, and substitute this into Eq. 1. We get, to first order in a,

$$\dot{a} = (\epsilon - 3gA_0^2)a = -2\epsilon a. \tag{3}$$

The perturbation $a(t)$ dies away if ϵ is positive, confirming our suspicion that the two solutions which appear at the bifurcation are stable. A bifurcation diagram illustrating

these results in shown in Fig. 1. This model corresponds to the existence of a featureless base state when the control parameter is below a certain point. At the bifurcation point, the base state loses stability and two new stable states (which are simply related by symmetry) with a nonzero pattern amplitude appear. Which of these two states actually occurs in a real system depends on initial conditions or experimental imperfections; in a perfect system they would both be equally probable.

One can apply linear stability analysis not only to simplified amplitude equations like Eq. 1, but also to the full equations of motion for any pattern-forming system. For Rayleigh-Bénard convection, this involves a few pages of algebraic manipulations of the Navier-Stokes equations, and one ends up with a stability boundary which gives the dimensionless control parameter R as a function of the wavenumber k. R, called the Rayleigh number, is proportional to the temperature difference across the layer. The treatment is slightly more complicated for electroconvection in smectic films, as described below, but the end result is again a stability boundary giving $R(k)$. The boundary calculated for the electroconvection problem [12] is plotted in Fig. 2. In this case, R turns out to be proportional to the square of the applied voltage. For one particular value of k, this boundary has a minimum, which gives both the control parameter R_c and the wavenumber k_c at the onset of the pattern state. The reduced control parameter ϵ, which appears in Eq. 1, is defined as $\epsilon = (R/R_c) - 1$. Near the minimum, the stability boundary is parabolic and $\epsilon_c(k) = \xi_0^2(k - k_c)^2$, where ξ_0 is a characteristic length scale.

The bifurcation illustrated in Fig. 1 is called a pitchfork or supercritical bifurcation, and is the analog of a second order phase transition in equilibrium thermodynamics. Eq. 1 is the same equation as that which describes second order transitions in the Landau theory of phase transitions, with the amplitude A corresponding to the order parameter. Just as in Landau theory, a breaking of up-down symmetry in the physical system leads to the introduction of a term proportional to A^2 into Eq. 1, and the bifurcation becomes subcritical, or equivalent to a first-order transition. In the context of equilibrium phase transitions the Landau equation is phenomenological and only valid in the mean-field limit,

when fluctuations can be neglected. Fluctuations cause the behaviour observed at real second-order phase transitions to be different in important ways from that predicted by, for example, the equivalent of Eq. 1. In contrast, fluctuations are usually completely negligible at pattern-forming transitions and the mean-field approximation is excellent. Equations similar to Eq. 1 can be derived rigorously from the full equations of motion for a number of pattern forming systems, including Rayleigh-Bénard convection and electroconvection in smectic films, as we shall see.

Linear analysis can give information about the location of bifurcation points and about the properties of the pattern at that point, but it breaks down when the amplitude of the pattern state is no longer infinitesimally small. To study the behaviour of the pattern above onset, one must take into account the nonlinearity of the governing equations. For example, the critical wavenumber k_c and the length scale ξ_0 are linear quantities, but the exponent of the nonlinear term in Eq. 1 and the sign and magnitude of the coefficient g are nonlinear quantities and can not be derived from a purely linear analysis.

One can study pattern formation in the weakly nonlinear regime using a type of perturbation theory. Close to onset, when the amplitude of the pattern is small and slowly varying in space and time, one can derive an equation for A. This has been done for only a small number of systems, including Rayleigh-Bénard convection [14,15] and, very recently, electroconvection in fluid films [13]. For one-dimensional patterns, the resulting amplitude equation in both cases is the Ginzburg-Landau equation,

$$\tau_0 \dot{A} = \epsilon A + \xi_0^2 \nabla^2 A - g|A|^2 A \tag{4}$$

where now A can in general be complex. The term in $\nabla^2 A$ allows for spatial variations in the pattern's amplitude and wave number. ξ_0 is the same length scale introduced above. τ_0 is a characteristic time scale, and is also a linear quantity. Eq. 4 will be familiar to anyone who has studied the Landau theory of superconductivity; in that case A is the order parameter and ξ_0 is the penetration depth.

Fig. 2 indicates that the convection pattern that appears at the bifurcation point can

exist over a range of wave numbers above onset. However, stability analysis of the pattern state above onset shows that it is not stable over the entire possible range. Rather, the range of stability is limited to a subset of the possible wavenumbers by a variety of instabilities. For Rayleigh-Bénard convection rolls, many of these involve two- or three- dimensional perturbations to the basic, one-dimensional pattern, and lead to, for example, modulations in the direction of the convection roll axes [16]. In purely one-dimensional patterns, however, there are two possible mechanisms that limit the range of stability close to onset. One is the Eckhaus instability, which is a long-wavelength instability of the phase of the pattern [17]. It leads ultimately to the creation or destruction of new pattern units if the wavelength gets too large or too small, respectively. The Eckhaus stability boundary near onset is parabolic and given approximately by $\epsilon_E = 3\epsilon_c$. The second mechanism requires the presence of boundaries, which, of course, must exist in any real system. The amplitude of the pattern must get small near a rigid boundary, due to the fact that the fluid flow velocity goes to zero there. This make it relatively easy to create or destroy rolls at the boundaries. This wavelength selection mechanism was studied theoretically by Cross et al. [18], who found that the range of wavenumbers stable against so-called end-selection was linear in ϵ, in contrast to the situation for the Eckhaus mechanism. This means that, close enough to onset, end-selection should have a narrower stability range than the Eckhaus instability and so should limit the stability range of a one-dimensional pattern.

The above discussion suggests that, at least in principle, pattern formation is quite well understood in the linear and weakly nonlinear regimes. The situation is quite different for the case of more strongly nonlinear patterns. When the nonlinearity is strong, very complex spatial and spatio-temporal behaviour can occur. An example is the spiral defect chaos state discovered recently in experiments on Rayleigh-Bénard convection in compressed gases [19]. A snapshot of this state is shown in Fig. 3; it has also been discussed in a recent article in *Physics in Canada* [20]. The convective flow pattern in the spiral defect chaos state is a continuously evolving collection of small interacting rotating spirals. Surprisingly, this state exists in a region of parameter space where the existing stability analysis indicated that

straight convection rolls were stable. It is now appreciated that both rolls and spiral defect chaos are stable, but that the chaotic state is the one reached from all but very special initial conditions [21].

In this highly nonlinear regime, amplitude equations and similar small-parameter expansion methods break down, and there are no well-established theoretical techniques to replace them. The most useful theoretical tool is large-scale computational simulation of various approximations to the equations of motion [22], which can confirm that the experimentally observed phenomena are indeed "in the equations," and can provide some insight into the relative importance of the various physical phenomena which contribute to the equations. It is not yet understood what the most important characteristics of such complex patterns are, and so it is not obvious what experimentalists should measure to properly characterize their dynamics. Thus beyond comparing the experimentally observed evolution and the computed evolution of the pattern, there is little understanding as to how to extend the close contact between theory and experiment that exists in the case of weakly nonlinear patterns, up to the strongly nonlinear regime.

Low-dimensional chaos, that is, chaos in systems with no or few spatial degrees of freedom, is well understood [23]. Complex spatiotemporally chaotic patterns like spiral defect chaos are observed in systems with many spatial degrees of freedom, i.e., systems with a size much larger than an appropriately defined correlation length of the pattern [1,24]. An important open question is whether there is any connection between spatiotemporal chaos and low-dimensional chaos, and if so, how we can extrapolate the tools used in the study of low-dimensional chaos to effectively study patterns such as spiral defect chaos. This question drives a great deal of recent experimental and theoretical work in the field of pattern formation [24].

Spiral defect chaos still retains some of the characteristics of the more ordered convection patterns: There is a reasonably well defined wavelength, and parts of the pattern look like they are not far from being straight convection rolls. However if the control parameter is increased to far above the convective onset, the flow becomes fully turbulent. Turbulence

has been studied extensively for decades, but remains poorly understood. The study of ordered flow patterns has led to the study of spatiotemporally chaotic patterns. Assuming we develop a coherent understanding of spatiotemporal chaos, can this then be extended and applied to fully developed turbulence? While the understanding of turbulence has always been one goal of much of the effort in nonlinear science, the answer to this question is unclear.

III. ELECTROCONVECTION IN FREELY SUSPENDED SMECTIC FILMS

We now consider a specific pattern-forming system, namely electrically driven convection in thin films of smectic liquid crystal. We have been using this system to study patterns both experimentally and theoretically for several years [8–13]. Although the instability which occurs in smectic films should exist in any sufficiently thin conducting fluid film, certain unusual physical properties of the liquid crystal medium make it ideal for the experiments we will describe. Thus, we exploit the properties of a soft material, the smectic, to study the convection pattern, which is the soft "nonequilibrium phase" of interest.

Liquid crystal molecules are anisotropic. Because of the possibility of orientational as well as positional ordering of the molecules, liquid crystals can exist in a variety of different physical phases [25]. The material used in our experiments is called 8CB, and has long, rod-shaped molecules, shown in Fig. 4(a). Some common phases of liquid crystals are illustrated schematically in Fig. 4(b–e). At high temperatures, the liquid crystal is isotropic (Fig. 4(b) — the orientation of the molecules is random, as is their position. As the temperature is lowered, however, the molecules can become orientationally ordered, although they remain positionally disordered, as in Fig. 4(c). This is the nematic phase, and the mean direction of orientation of the molecules is called the director. The material is still fluid, but has anisotropic properties. It is this phase which is most commonly used in liquid crystal display devices. Further decreasing the temperature leads to the appearance of some positional order in addition to the orientational order. In the smectic-A phase, Fig. 4(d), the molecules

arrange themselves into layers, with the director pointing parallel to the layer normal. The material is still fluid, with no positional ordering within the individual layers, so this phase has orientational order and one-dimensional positional order. The smectic-C phase is similar except that the director points at an angle to the layer normal. Many other more exotic smectic phases exist which are characterized by various degrees of positional ordering within the smectic layers.

From the point of view of our experiments, the key features of the smectic-A and C phases are the following: Smectics are layered materials, and for the A and C phases there is no positional order within the layers. Flow between layers is much more difficult than flow within the layers. Because of their layered structure, smectics easily form very thin suspended films, i.e., films with two free surfaces, like soap bubbles. A thin film of smectic-A material behaves, at least from the hydrodynamic point of view, as a two-dimensional isotropic liquid. Energy considerations make the formation of partial layers unfavorable and so it is possible to make smectic films which are uniformly an integer number of molecular layers thick, and which remain so despite the presence of vigorous hydrodynamic flow in the layer planes. Similar considerations apply to smectic-C films, except that in this case the flow can couple to the orientation of the molecules and a film behaves as an anisotropic two-dimensional fluid. Our discussion here will concern experiments with the simpler smectic-A phase; smectic-C is the subject of some of our current work.

The smectic film forms a nearly ideal two-dimensional fluid which can be driven into convection. Since the thickness of our films is extremely small (from 60 to 3000 Å), three-dimensional effects are unimportant, and in particular the various two- and three-dimensional instabilities to which Rayleigh-Bénard convection rolls are subject do not affect the flow pattern which develops in this system. Thus smectic films are a very clean system for the study of one-dimensional patterns, i.e., patterns which are characterized by spatial periodicity along a single direction.

Our experimental apparatus is shown in Fig. 5. The smectic film itself is typically 2 mm wide and 20 mm long. It is supported by a film holder consisting of two 25 μm diameter

tungsten wires along the long sides, and two thin plastic "wipers" along the short sides. One of the wipers is movable via a motor-driven micrometer screw. The film's top and bottom surfaces are in contact with the air. The tungsten wires also serve as electrodes, as described below. The film holder is enclosed in a temperature controlled, grounded aluminum box, which is labeled "liquid crystal cell" in Fig. 5. The film is optically accessible from above and below.

A film is made by bringing the wipers together, putting a small droplet of liquid crystal on the place where they join, and then slowly moving the wipers apart. The film which forms is usually quite nonuniform in thickness, but with practice one can manipulate the film to get it perfectly uniform in thickness over its entire area. The film thickness is measured optically. The reflectivity of a thin film depends on the film thickness, as does its colour when it is viewed in reflected white light. Using a combination of reflectivity measurements using the laser shown in Fig. 5, and observations of the film colour, we can measure film thicknesses exactly for very thin films, and to within ± 1 layer for films between 10 and 100 layers thick.

When a dc voltage V is applied across the film, there is a well-defined critical voltage at which a flow pattern develops. The flow consists of a one-dimensional pattern of counter-rotating vortices which fill the length of the film. This can be observed qualitatively in a nonuniform film: different thicknesses appear as different colours in reflected light, and any thickness variations are advected by the flow. This results in a beautiful swirling of colours, as illustrated on the cover of this issue. For quantitative measurements, however, we use only uniformly thick films. In this case, we visualize the flow by dusting the film with small particles (chalk dust was used in our earlier work; we have now graduated to using incense smoke). The particles are advected by the flow, and by tracking them over time we can measure the flow pattern and the velocity field. Fig. 6(a) is a photograph of a convecting film well above onset. The film was illuminated from below by a light source chopped at a known frequency. The streaks show the paths of the flow visualization particles. A vector plot of the velocity data extracted from this photograph is shown in Fig. 6(b). The

measured velocity field is well described by the first few terms of an expansion in terms of eigenfunctions which satisfy the boundary conditions at the electrodes [9]. This result implies that a description of the nonlinear pattern via amplitude equations will be a good approximation.

We measured the voltage at which the flow pattern appears as a function of film thickness for films as thin as 2 molecular layers thick [11]. The onset voltage V_c increases linearly with film thickness as shown in Fig. 7. The inset to Fig. 7 shows the maximum in the flow velocity as a function of the control parameter ϵ, which for this system is given by $\epsilon = (V/V_c)^2 - 1$. While there is a small amount of rounding at the transition due to experimental imperfections, the transition is quite sharp. Fits to the data indicate that the flow velocity increases like $\epsilon^{1/2}$, just as for the pitchfork bifurcation illustrated in Fig. 1, and as predicted by the Ginzburg-Landau equation derived for this system, Eq. 4. We have also measured the spacing of the vortices just above onset. This gives the critical wavenumber k_c of the pattern, which was found to be $(4.94 \pm 0.25)/d$, where d is the film width, independent of thickness [8,11].

These results can be compared with the results of a theoretical stability analysis for this system [12,13]. The linear stability analysis in this case [12] involves a combination of fluid dynamics and electrostatics. The fluid dynamical part of the problem is two dimensional, but the electrostatic part is three dimensional. First, the distribution of charges in the film in the no-flow state is calculated. The result is a "charge inversion" analogous to the density inversion found in Rayleigh-Bénard convection, i.e., there is an excess of positive charge near the positive electrode, and an excess of negative charge near the negative electrode. This charge density is purely a consequence of the electrostatic boundary conditions that apply at the surface of any current-carrying conductor. As in Rayleigh-Bénard convection, this inversion is potentially unstable, and it is the viscosity and conductivity of the film which prevent the onset of flow for arbitrarily small applied voltages. Once this "base state" is known, we can look at its stability to small perturbations. The resulting stability boundary was shown above in Fig. 2; here R is a dimensionless version of the control parameter that

depends on the fluid properties and is proportional to the square of the applied voltage. The minimum in the stability curve defines the onset voltage and the wavenumber of the pattern at onset. Arguments similar to those used above suggest that the vortex size should be on the order of the film width d, and the theoretical value of k_c is $4.744/d$. The result for the onset voltage is

$$V_c = \frac{s}{\epsilon_0}\sqrt{\sigma \eta R_c} \tag{5}$$

where s is the film thickness, σ the conductivity, η the viscosity, and ϵ_0 the permittivity of free space. R_c is the value of R at the minimum in the stability curve, which we have calculated numerically to be 76.77 for infinitely thin wire electrodes [12].

The results of the linear stability analysis are in good agreement with the experimental results. In particular, the experimental and theoretical values of k_c agree within the experimental error (which is mostly due to uncertainties in the measurement of d), and the theoretically predicted linear increase in V_c with thickness is confirmed experimentally for small s. The slope of the experimental $V_c(s)$ data is somewhat higher than the theoretical prediction, but there are large uncertainties in the values of the fluid properties for 8CB, and the effect of air drag, which we expect to be important for thin films, has not been taken into account in the theory.

We have also derived the Ginzburg-Landau equation, Eq. 4, from a weakly nonlinear analysis of the full electrohydrodynamic equations of motion for this system [13]. This equation describes the behaviour of the pattern slightly above onset. We have already seen that the flow amplitude increases above onset like $\epsilon^{1/2}$, in agreement with the predictions of Eq. 4, and the value of the nonlinear coefficient g can be determined from fits to the data.

There are other predictions of the GLE which can be tested. For example, the flow amplitude must go to zero at the rigid ends of the film. If we let x be the coordinate parallel to the electrodes, and solve Eq. 4 with the boundary condition $A = 0$ at $x = 0$ we get $A = A_0 \tanh(x/2^{1/2}\xi)$, where $A_0 = (\epsilon/g)^{1/2}$ is the convective amplitude far from the end walls. ξ is the length scale over which the pattern's amplitude grows from its value of 0 at

the walls to the bulk value, and is given by $\xi = \xi_0/\epsilon^{1/2}$; ξ diverges at $\epsilon = 0$. Experimental measurements of the pattern amplitude as a function of distance from the ends of the film results are in excellent agreement with these predictions, and give $\xi_0 = (0.36 \pm 0.02)d$. This is about 20% larger than the value obtained from the theory.

We can also study the dynamics of the system. If the control parameter ϵ is suddenly changed, Eq. 4 predicts that the amplitude of the pattern will evolve with time according to

$$A(t) = \left(\frac{(\epsilon A_i^2/g)e^{2t/\tau}}{(\epsilon/g) - A_i^2(1 - e^{2t/\tau})} \right)^{1/2} , \tag{6}$$

where A_i is the initial value of the amplitude, and ϵ here is the final value of the control parameter. The time scale τ is equal to τ_0/ϵ and, like the length scale ξ, diverges at the onset of convection. Fig. 8 shows values of the amplitude of the flow pattern measured following a step in ϵ. The curves are fits to the prediction of Eq. 6, with ϵ/g, A_i, and τ used as fitting parameters, and fit the data very well. Values of τ obtained from a number of similar fits for different values of ϵ show the predicted $1/\epsilon$ divergence. We cannot yet make a detailed comparison between the experimental and theoretical values for τ_0 and g, since they are calculated in terms of the fluid properties, which are not very accurately known.

Finally we discuss wavenumber selection above the onset of convection. As discussed in Section II, there are two possible mechanisms by which adjustments of the wavenumber of our one-dimensional patterns can take place. One is the Eckhaus instability, and the other is the end-selection mechanism. The stability boundaries for the two mechanisms are predicted to be quite different. The range of stable wavenumbers of our vortex pattern was measured in two ways [10]. In the first set of experiments, a pattern of a particular wavenumber was prepared at a particular value of ϵ. Then the length of the film was changed by moving the motor-driven wiper which supported one end of the film. Somewhat remarkably, the film thickness remained constant during this process. The smectic layers are very resistant to defects, and the excess material required to maintain the film's thickness is simply drawn into the existing layers from (or goes from the film into) wetting layers on the wipers and the

electrodes. As the length of the film increased, the number of vortices remained constant as long as the pattern remained stable, and so the pattern's wavelength $\lambda = 2\pi/k$ increased. Eventually, however, the wavelength got so large that the pattern became unstable. When this happened a new vortex formed at the one end of the film, and the wavelength of the pattern dropped back into the stable region. Similarly when the film length was decreased, the wavelength decreased until the pattern reached the low-wavelength limit of its stability, at which point a vortex disappeared at one end of the film, raising the wavelength back into the stable band. In the second set of experiments, ϵ was varied at constant film length. Again there were limits at which the pattern became unstable resulting in the gain or loss of vortices at the ends of the film.

The stability boundary close to the onset of convection measured in this way is shown in Fig. 9 [10]. The lower dotted curve is the calculated linear stability boundary, and the upper dotted curve is the approximate Eckhaus boundary. The measured stability boundary lies well inside the Eckhaus boundary, and the stability range increases approximately linearly with increasing ϵ, as predicted for the end-selection mechanism [18]. Although this mechanism was predicted 15 years ago, it had not previously been clearly observed in experiments because of the influence of three-dimensional effects [26]. Because our films are extremely thin, such effects are completely negligible, and the one-dimensional end-selection mechanism is the dominant wavenumber selection process, as predicted theoretically.

IV. DISCUSSION

A small number of fluid dynamical systems have become paradigms for the study of patterns away from equilibrium. Rayleigh-Bénard convection is one of these standard systems. In that case, a comprehensive nonlinear theoretical analysis exists [16], and experiments are performed with such precision that the agreement between experiment and theory is sometimes on the level of 0.1% [7]. Despite this, Rayleigh-Bénard convection still produces surprises — the recent discovery of spiral defect chaos is one example — and will continue

to be a useful testing ground as the study of patterns is extended further into the nonlinear regime.

Rayleigh-Bénard convection is an exception, however, and most experimental systems have been much less thoroughly studied. The level of our understanding of electroconvection in smectic films is substantially below that of Rayleigh-Bénard convection, but nonetheless we are getting close to the point of quantitative agreement between theory and experiment both at the pattern onset and in the weakly nonlinear regime above onset. The largest uncertainties arise due to poorly known fluid properties, as many of the fluid properties of liquid crystals have not been accurately measured.

Our work on this system is continuing in several directions. As ϵ is increased above onset, the flow pattern undergoes a transition to a state of unsteady flow, in which local flow velocities vary erratically in time. This transition appears to be the result of a secondary instability of the vortex pattern. This is particularly interesting because most of the secondary instabilities that have been identified in Rayleigh-Bénard convection involve reorientation of the roll axes, a process which is not possible in smectic films. Thus, the unsteady flow regime may be an interesting spatiotemporally chaotic state reached via a new sort of instability. We are currently studying this state in rectangular films.

We are also studying electroconvection patterns in films in which the driving voltage is applied between the inner and outer edges of an annular film holder. A version of this experiment using a nonuniformly thick film was shown on a recent *Physics in Canada* cover [27]. Such a film has periodic boundary conditions, in contrast to the rigid end conditions in our rectangular films, and this should affect the stability boundary of the pattern. This geometry also makes it possible to quantitatively study the current-voltage characteristics of the film because no current leaks around the ends of the film. When the film is convecting it carries more current, and this excess is sensitive to global features of the pattern. We are also looking at the behaviour of the pattern in annular films when the film is sheared by rotating the inner edge of the annular film holder. The rate of shear gives a second independent control parameter, other than the applied voltage. The shear breaks the reflection symmetry

of the base state and the onset of convection becomes hysteretic. The pattern consists of traveling, rather than stationary vortices. Intersting unsteady flow states are also found in this system when the inner electrode is moved off-centre, forming an eccentric annular film.

We are also investigating the development of similar patterns in smectic-C liquid crystals. In this case, the director is inclined at an angle to the film plane, and can be reoriented by the flow [28]. The resulting flow alignment can be observed in polarized light. These experiments may provide a probe of some interesting liquid crystal physics as well as further studies of the flow pattern. On the theoretical side, we are extending our existing linear and weakly nonlinear analyses to the annular case. We also hope to be able to develop the nonlinear stability theory necessary to understand the wavenumber selection process in rectangular and annular films.

Convection patterns in smectic films are extremely simple examples of nonlinear pattern formation under nonequilibrium conditions. Indeed, the system was deliberately chosen for its simplicity. A great gulf separates this model laboratory system from the vast complexity of the natural world. Yet even this simple system exhibits many nonlinear phenomena which are challenging to explain. If nothing else, this serves to remind us how little we know about nonequilibrium physics.

V. ACKNOWLEDGEMENTS

This research was supported by the Natural Sciences and Engineering Research Council of Canada, and performed in collaboration with A.D. May, S.S. Mao, Z.A. Daya, T.C.A. Molteno, and V. B. Deyirmenjian.

VI. APPENDIX — A SHORT ANNOTATED BIBLIOGRAPHY

While the relevant technical papers have been included in the references, interested readers looking for a deeper introduction to the field of pattern formation, and to nonlinear science in general, will find the following references useful.

There are many textbooks that deal with low-dimensional chaos and other aspects of nonlinear science, but few that include pattern formation. Two good recent texts on pattern formation are

- G. Nicolis, *Introduction to Nonlinear Science*, (Cambridge University Press, Cambridge, 1995)
- P. Manneville, *Dissipative Structures and Weak Turbulence* (Academic, San Diego, 1990)

with the latter being rather heavier mathematically.

Some good textbooks covering chaos and other aspects of nonlinear dynamics, but with not much discussion of pattern formation, are

- G.L. Baker and J.P. Gollub, Chaotic Dynamics: an introduction (Cambridge University Press, Cambridge, 1996)
- S. Strogatz, Nonlinear Dynamics and Chaos (Addison-Wesley, Reading, 1994).
- E. Infeld and G. Rowlands, Nonlinear Waves, Solitons and Chaos (Cambridge University Press, Cambridge, 1990)

The book by Baker and Gollub is a particularly straightforward introduction at the undergraduate level.

A good book on hydrodynamic instabilities is

- P.G. Drazin and W.H. Reid, Hydrodynamic Stability (Cambridge University Press, Cambridge, 1991)

and the classic (and very readable) text on the subject is

- S. Chandrasekhar, Hydrodynamic and Hydromagnetic Stability (Oxford University Press, London, 1961)

There are several review papers on aspects of pattern formation, many of which deal with Rayleigh-Bénard convection. These include

- G. Ahlers, in Lectures in the Sciences of Complexity, edited by D. Stein (Addison-Wesley, Reading, 1989), p. 175,

a very nice review of experimental work on Rayleigh-Bénard convection and Taylor vortex flow, emphasizing the analysis of experimental results in terms of the Ginzburg-Landau equation,

- V. Croquette, Contemp. Phys. **30**, 113 (1989); **30**, 153 (1989),

a review of experiments on convection in compressed gases,

- F. Busse, in Hydrodynamic Instabilities and the Transition to Turbulence, edited by H.L. Swinney and J.P. Gollub (Springer-Verlag, Berlin, 1981), p. 97,

which is a review of the detailed nonlinear analysis of Rayleigh-Bénard convection carried out by Busse and co-workers, and

- J.R. de Bruyn, E. Bodenschatz, S.W. Morris, S.P. Trainoff, Y. Hu, D.S. Cannell, and G. Ahlers, Rev. Sci. Instrum. **67**, 2043 (1996)

a review of Rayleigh-Bénard convection in compressed gases, emphasizing the experimental design.

An excellent comprehensive and detailed review of the theory of pattern formation can be found in

- M.C. Cross and P.C. Hohenberg, Rev. Mod. Phys. **65**, 851 (1993).

Finally, references to more recent ideas on spatiotemporal chaos may be found in

- M.C. Cross and P.C. Hohenberg, Science, **263** 1569 (1994).

Our own work on electroconvection in smectic films is described in the following papers, most of which can be downloaded from http://mobydick.physics.utoronto.ca:

- S.W. Morris, J.R. de Bruyn, and A.D. May, Phys. Rev. A **44**, 8146 (1991),

which deals with measurements of the convective velocity field,

- S.S. Mao, J.R. de Bruyn, Z.A. Daya, and S.W. Morris, Phys. Rev. E **54**, R1048 (1996),

on wavenumber selection,

- S.S. Mao, J.R. de Bruyn, and S.W. Morris, Physica A, to be published,

on the analysis of experimental results using the Ginzburg-Landau equation, and

- Z.A. Daya, S.W. Morris, and J.R. de Bruyn, Phys. Rev. E **55**, 2682 (1997).

- V.B. Deyirmenjian, Z.A. Daya, and S.W. Morris, Phys. Rev. E, to be published,

which describe the linear and weakly nonlinear stability analysis for this system.

REFERENCES

[1] M.C. Cross and P.C. Hohenberg, Rev. Mod. Phys. **65**, 851 (1993).

[2] G. Nicolis, *Introduction to Nonlinear Science*, (Cambridge University Press, Cambridge, 1995)

[3] Q. Ouyang and H.L. Swinney, Chaos **1**, 411 (1991).

[4] J.R. de Bruyn, Cold Regions Sci. Tech., to be published.

[5] I. L'Heureux, Phys. Rev. E **48**, 4460 (1993).

[6] K.J. Lee, E.C. Cox, and R.E. Goldstein, Phys. Rev. Lett. **76**, 1174 (1996).

[7] G. Ahlers, in *Lectures in the Sciences of Complexity,* edited by D. Stein (Addison-Wesley, Reading, 1989), p. 175.

[8] S.W. Morris, J.R. de Bruyn, and A.D. May, Phys. Rev. Lett. **65**, 2378 (1990); J. Stat. Phys. **64**, 1025 (1991).

[9] S.W. Morris, J.R. de Bruyn, and A.D. May, Phys. Rev. A **44**, 8146 (1991).

[10] S.S. Mao, J.R. de Bruyn, Z.A. Daya and S.W. Morris, Phys. Rev. E, **54**, R1048 (1996).

[11] S.S. Mao, J.R. de Bruyn, and S.W. Morris, Physica A, to be published.

[12] Z.A. Daya, S.W. Morris, and J.R. de Bruyn, Phys. Rev. E **55**, 2682 (1997).

[13] V.B. Deyirmenjian, Z.A. Daya, and S.W. Morris, Phys. Rev. E, to be published.

[14] A.C. Newell and J.A. Whitehead, J. Fluid Mech. **38**, 279 (1969).

[15] L.A. Segel, J. Fluid Mech. **38**, 203 (1969).

[16] F. Busse, in Hydrodynamic Instabilities and the Transition to Turbulence, edited by H.L. Swinney and J.P. Gollub (Springer-Verlag, Berlin, 1981), p. 97.

[17] V. Eckhaus, *Studies in Nonlinear Stability Theory*, (Springer-Verlag, Berlin, 1965).

[18] M.C. Cross, P.G. Daniels, P.C. Hohenberg, and E.D. Siggia, Phys. Rev. Lett. **45**, 898 (1980); J. Fluid Mech. **127**, 155 (1983).

[19] S.W. Morris, E. Bodenschatz, D.S. Cannell, and G. Ahlers, Phys. Rev. Lett. **71**, 2026 (1993).

[20] S.W. Morris, E. Bodenschatz, and J.R. de Bruyn, Physics in Canada **50**, 9 (1994).

[21] S.W. Morris, E. Bodenschatz, D.S. Cannell, and G. Ahlers, Physica **D 71**, 164 (1996).

[22] W. Decker, W. Pesch, and A. Weber, Phys. Rev. Lett. **73**, 648 (1994).

[23] S. Strogatz, Nonlinear Dynamics and Chaos (Addison-Wesley, Reading, 1994).

[24] M.C. Cross and P.C. Hohenberg, Science, **263** 1569 (1994).

[25] P.G. de Gennes and J. Prost, *The Physics of Liquid Crystals* (Clarendon, Oxford, 1993).

[26] B. Martinet, P. Haldenwang, G. Labrosse, J.C. Payan, and R. Payan, in *Cellular Structures in Instabilities*, edited by J.E. Wesfreid and S. Zaleski (Springer-Verlag, Berlin, 1984), p. 33.

[27] Physics in Canada, July 1993.

[28] A. Becker, S. Ried, R. Stannarius and H. Stegemeyer, Europhys. Lett., to be published.

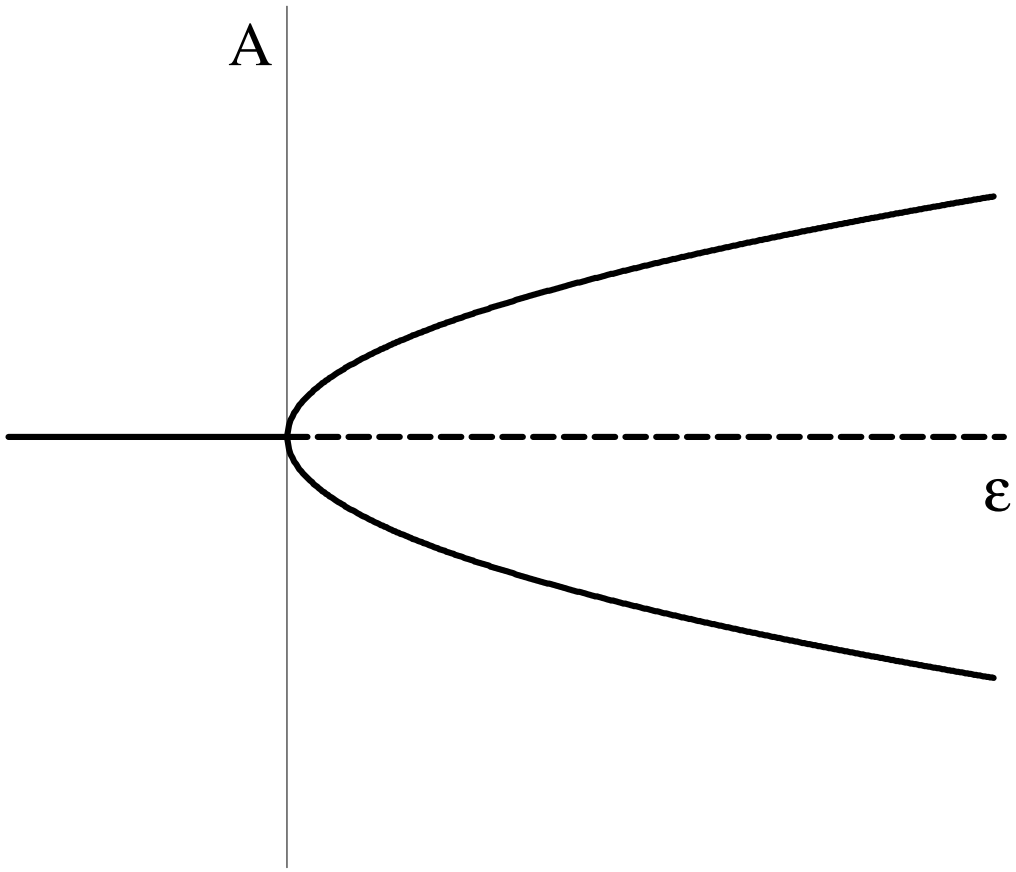

FIG. 1. Bifurcation diagram for the Landau equation, $\dot{A} = \epsilon A - gA^3$. Solid lines represent stable solutions and the dashed line represents an unstable solution.

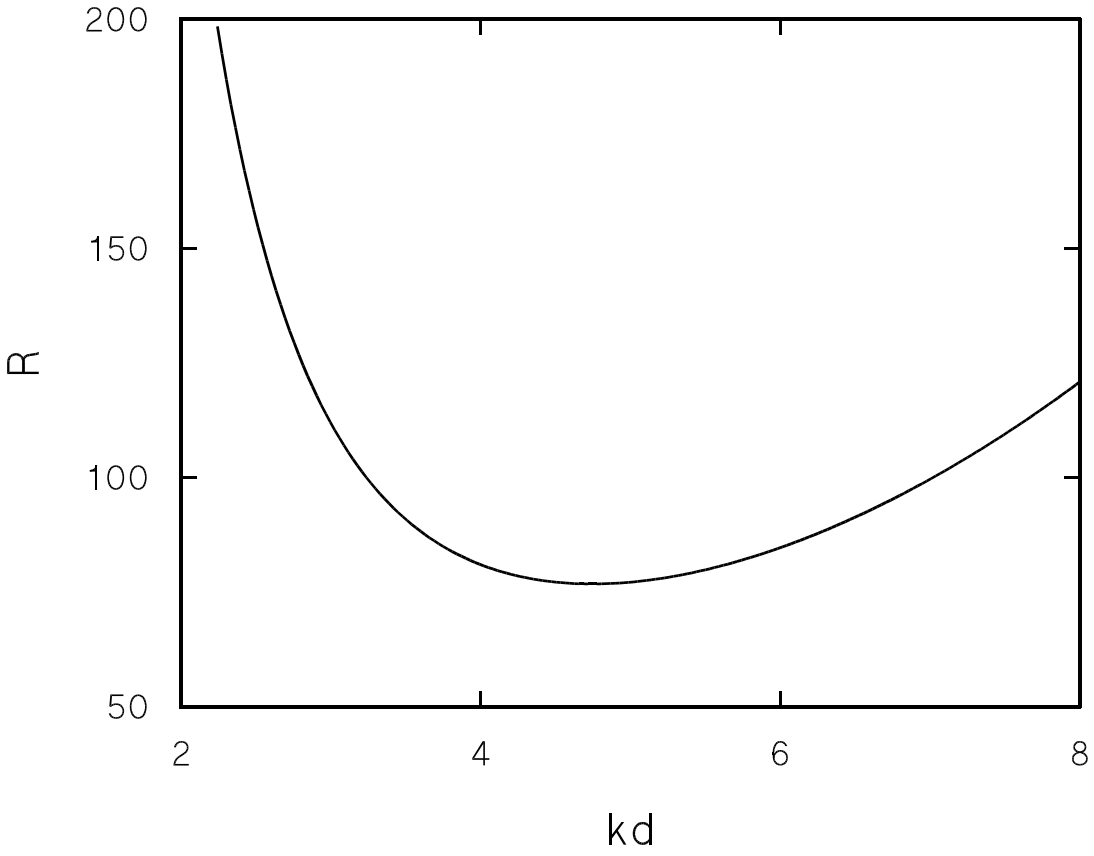

FIG. 2. Linear stability boundary for electroconvection in a fluid film, plotted in terms of the wavenumber k of the convection pattern and the dimensionless control parameter R, which in this case is proportional to the square of the voltage applied across the film. The onset of convection occurs at the minimum of the curve.

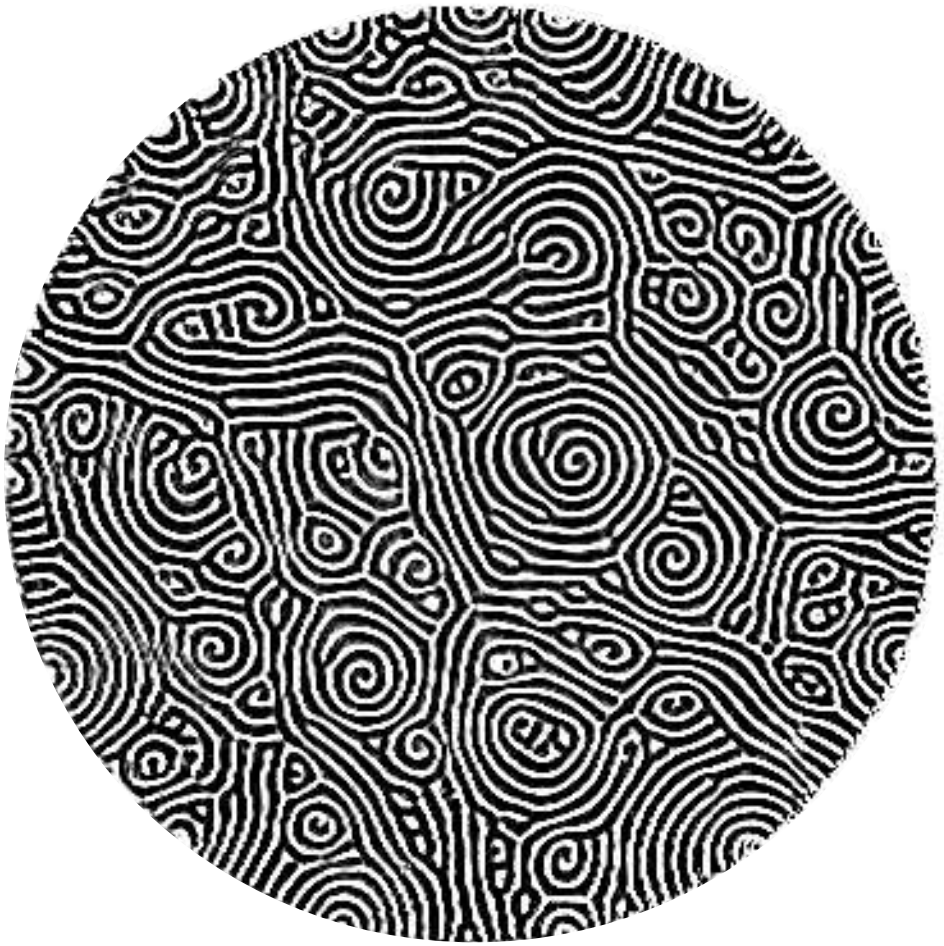

FIG. 3. A snapshot of spiral defect chaos in Rayleigh-Bénard convection in compressed CO_2, imaged using shadowgraphy. The pattern evolves continuously with time.

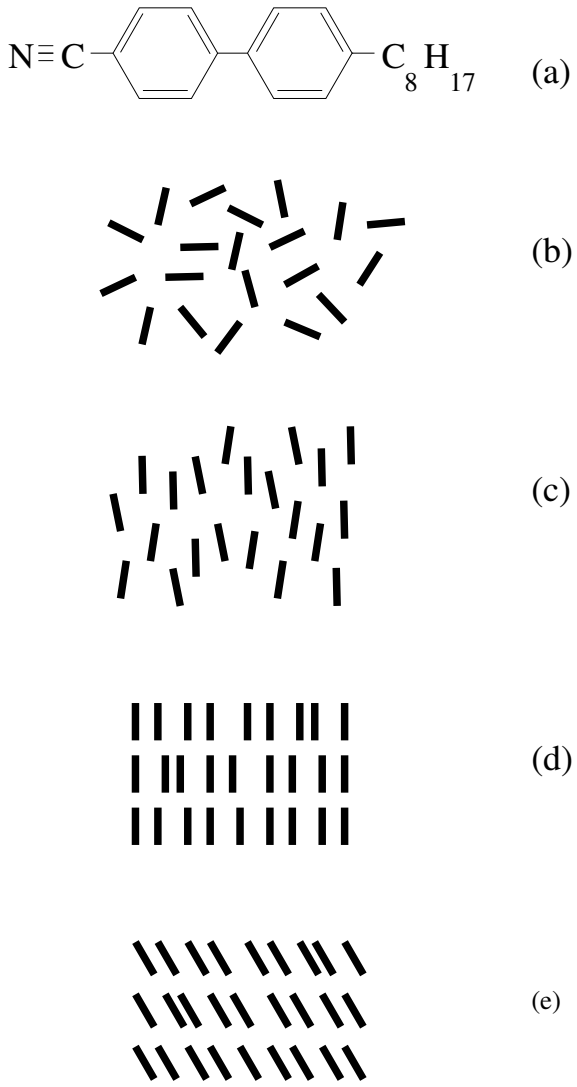

FIG. 4. (a) The liquid crystal 8CB used in our experiments. The rod-shaped molecule is approximately 30 Å long. (b)–(e) Schematic illustration of the structure of various liquid crystal phases: (b) isotropic; (c) nematic; (d) smectic-A; (e) smectic-C. The experiments described in this paper were performed on films of 8CB in the smectic-A phase.

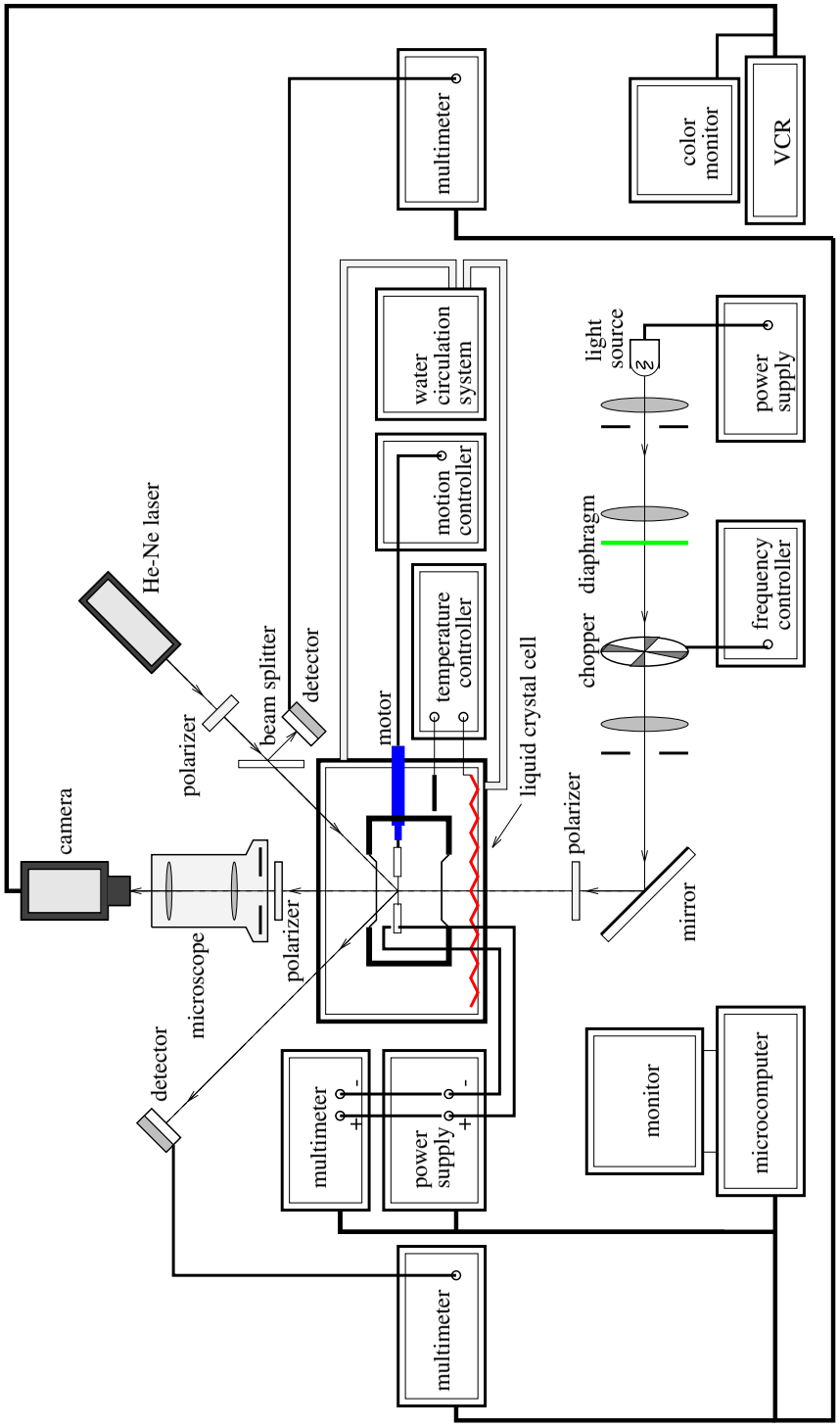

FIG. 5. Experimental apparatus for the study of pattern formation in freely-suspended smectic films.

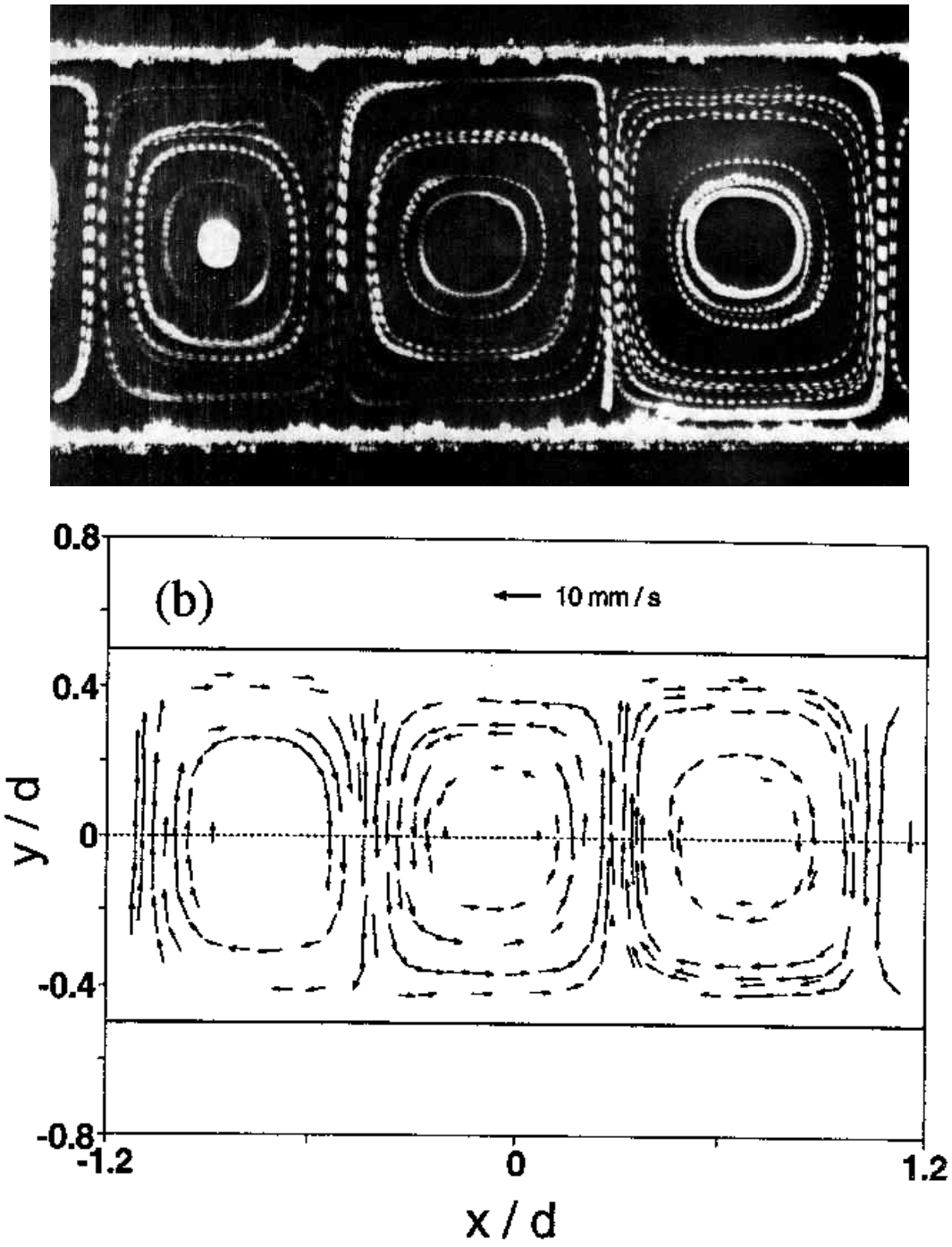

FIG. 6. (a) A time exposure of a convecting smectic film. The illumination was chopped at a known frequency, and the streaks show the paths followed by the flow visualization particles. (b) The velocity field extracted from (a).

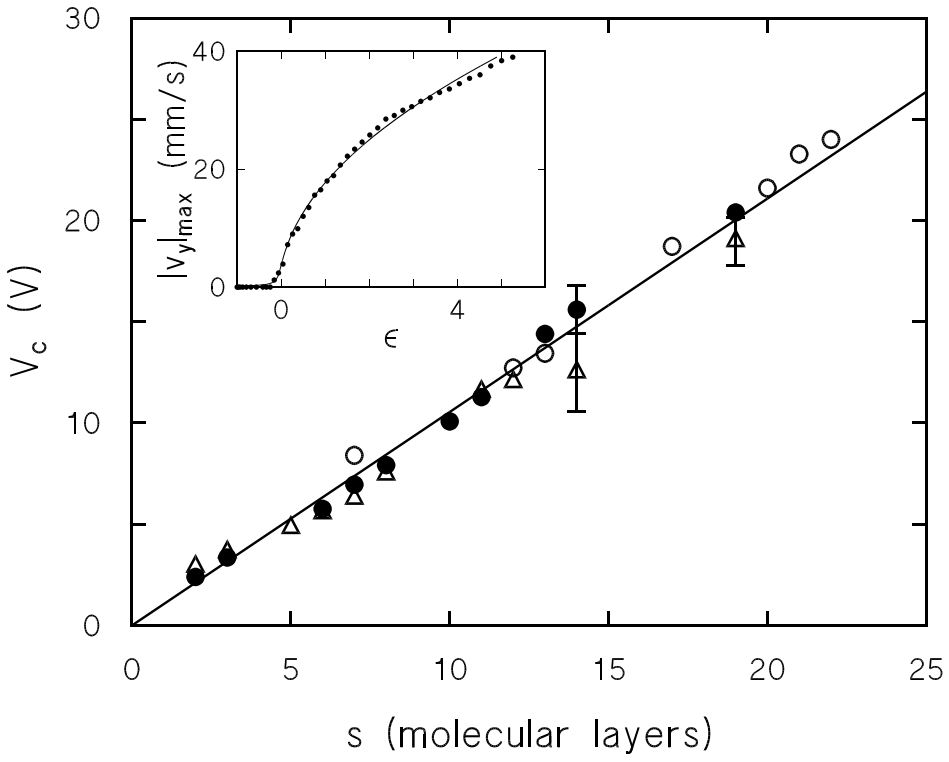

FIG. 7. The voltage across the film at the onset of convection, as a function of the film thickness. One molecular layer is 3.16 nm thick. The inset shows the amplitude of the convective flow velocity as a function of $\epsilon = (V^2 - V_c^2)/V_c^2$.

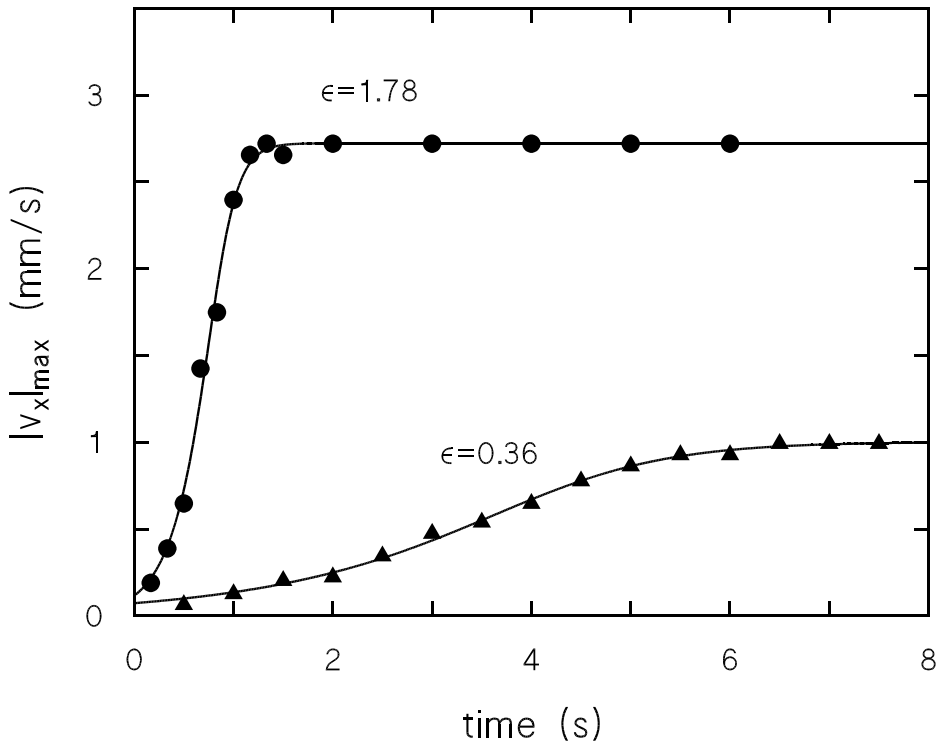

FIG. 8. The evolution of the pattern amplitude after a sudden change in the voltage across the film, for two different final values of ϵ. The curves are fits to the functional form predicted by the Ginzburg-Landau equation, Eq. 4. The film was 20 molecular layers thick.

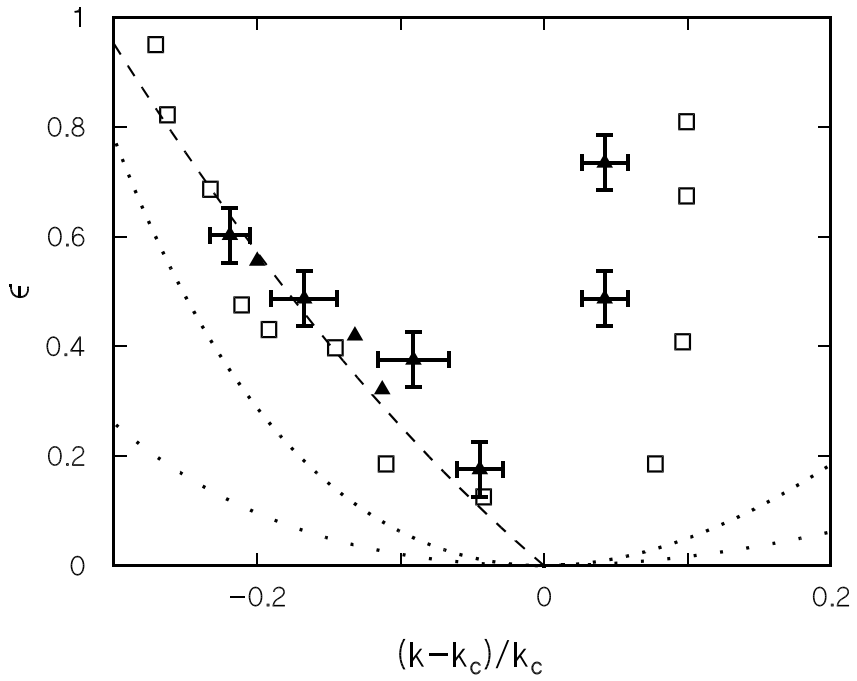

FIG. 9. The stable wavenumber range for electroconvection in smectic films close to onset. The solid symbols were determined by increasing (circles) or decreasing (triangles) the applied voltage at constant film length. The open squares were determined by varying the film length at constant voltage. The lower and upper dotted lines are the calculated linear stability boundary and the Eckhaus boundary, respectively. The dashed line is a fit of the experimental data for $\epsilon < 1$, $k < k_c$ to the linear form predicted theoretically, with a quadratic correction term.